Scanning Microscopy

Volume 3 | Number 2 Article 7

7-13-1989

Processing of Particle Induced X-Ray Emission (PIXE) Spectra Contrasted with Electron Probe Microanalysis

J. L. Campbell
University of Guelph

Scanning Microscopy, Vol. 3, No. 2, 1989 (Pages 449-459) 0891-7035/89$3.00+.00
Scanning Microscopy International, Chicago (AMF O'Hare), IL 60666 USA

PROCESSING OF PARTICLE INDUCED X-RAY EMISSION (PIXE) SPECTRA CONTRASTED WITH ELECTRON PROBE MICROANALYSIS

J.L. CAMPBELL*

Guelph-Waterloo Program for Graduate Work in Physics,
University of Guelph, Guelph, Ontario
Canada N1G 2W1

(Received for publication March 23, 1989, and in revised form July 13, 1989)

Abstract

PIXE (proton-induced X-ray emission) analysis and EPMA (electron probe microanalysis) give rise to similar energy-dispersive X-ray spectra, and so the processing of these spectra has common elements. Consequently approaches developed for EPMA may be of use in PIXE, one example being methodology for removing the continuous background. However various special aspects of PIXE result in a somewhat more complex problem. The range of X-ray energies of interest is wider and K X-rays of medium atomic number elements tend to be used where EPMA would rely upon their L X-rays; since the projectile penetration is much greater, matrix corrections are larger; due to PIXE's lower detection limits the range of peak heights in a given spectrum can be much greater and the influence of low-energy tailing on intense X-ray peaks becomes more important. Approaches taken to spectrum processing in PIXE reflect these aspects, and a variety of approaches have been developed which assure accurate extraction of peak intensities.

KEY WORDS: Proton-induced X-ray emission; energy-dispersive X-ray microanalysis, spectrum fitting.

*Address for correspondence:
J.L. Campbell,
Guelph-Waterloo Program for
Graduate Work in Physics,
University of Guelph,
Guelph, Ontario, Canada N1G 2W1.
Phone No. (519) 824-4120 x3125.

Introduction

Electron probe micro-analysis (EPMA) and proton-induced X-ray emission analysis (PIXE) employing energy-dispersive X-ray spectroscopy with Si(Li) detectors give rise to similar challenges as regards extracting accurate intensities of characteristic X-ray peaks from the measured spectra. Energy-dispersive X-ray spectra have low energy resolution and so there are often complicated peak overlaps. The characteristic peaks are superimposed on bremsstrahlung backgrounds whose energy-dependence is strong at low energies. On the EPMA side, this problem has been pursued for a long period and reliable software for fitting spectra is available, some of it on a commercial basis. In the newer PIXE technique, developments in spectrum fitting have tended to flow from the earlier gamma-ray spectroscopy experience of many PIXE proponents rather than as a natural extension of available EPMA experience. More recently however, as recognition has grown of the complementary nature of EPMA and micro-PIXE, more advantage has been taken in PIXE and micro-PIXE of approaches originally developed for EPMA. PIXE has now reached the stage where several extensive software packages are commercially available.

In EPMA, in situations where the resolution of energy-dispersive X-ray spectroscopy (EDX) is a stumbling-block, it is often possible to turn directly to wavelength-dispersive X-ray spectroscopy (WDX) to solve the problem; the main requirement is that the specimen withstand the increased beam intensity necessitated by the concomitant loss of geometric efficiency. In micro-PIXE, the beam currents are limited to typically $\lesssim$1 nA, and in the case of trace element work where counting statistics are at a premium, the option of a change to WDX does not present itself; WDX could be feasible for the major elements comprising the matrix but not for trace elements at ppm concentrations. This limitation of PIXE to the energy-dispersive mode renders accurate spectral processing all the more important.

The object of this paper is to explore in tutorial fashion the common aspects of the extraction of peak intensities from EDX spectra in EPMA and micro-PIXE. In order to maintain this theme we shall avoid diversion into detail, providing instead simple examples and appropriate

literature references where details may be found. The special problems that arise in PIXE will be emphasized.

X-ray spectra are generally fitted to a model, using either linear or non-linear least-squares methodology. The model contains numerical or analytical descriptions of the characteristic X-ray lines and usually also of the background continuum; sometimes the alternative of removing the background from the raw data by a mathematical operation is adopted. The spectra discussed here are taken from specimens thick enough to stop the beam and therefore requiring allowance for matrix effects. Use of such specimens has been the norm in EPMA, whereas in PIXE's early stages the technique was limited to thin film specimens. Now that PIXE has matured to the stage at which specimens thick enough to stop the beam are analyzed routinely, there is a complete analogy between the two techniques. The only salient differences are that with PIXE the analyzed depth is some ten times greater and the detection limits (using EDX in both cases) often more than ten times lower.

Spectral Regions

In EPMA the X-ray energy region of interest is essentially 0.5-15 keV. With typical electron energies of 10-30 keV, it is not possible to excite the K X-rays of high Z elements; for medium Z the electron energy is close enough to the K binding energy that ionization cross-sections are rather low. For these reasons it is customary to rely on the M X-rays of high Z elements, the L X-rays for medium Z (i.e., $30 \leq Z \leq 60$) and the K X-rays for elements of $Z \leq 30$.

In PIXE the situation is very different since the MeV proton energies required to attain sufficient ionization cross-sections are far above the various K, L and M binding energies. It is customary to use K X-rays for elements of Z up to 55, and L X-rays for $Z > 55$. Frequently the use of K X-rays confers the advantage that the peaks of interest lie at energies outside the main bremsstrahlung region. A crude but useful expression for the bremsstrahlung end-point energy in PIXE is $0.002\ E_p$, where E_p is the proton energy. By way of example Figure 1 shows the calculated PIXE peaks (ignoring detector resolution) for a pyrrhotite (FeS) mineral containing silver and selenium each at 100 ppm concentration. In this case EPMA would normally rely upon the silver L X-rays, which of course are superimposed on the electron bremsstrahlung. PIXE's use of the silver K X-rays is advantageous not just because they are well separated from the main bremsstrahlung region (0–6 keV) but because they are also well separated from K and L X-rays of iron. Another advantage is the much smaller attenuation and more accurately known attenuation coefficients of the higher-energy silver K X-rays in the matrix.

EPMA has the advantage that as the beam energy is lowered towards 10 keV the iron K X-ray yield decreases. In PIXE, the very high counting rate of matrix X-rays necessitates use of a 0.1–1.0 mm aluminum absorber to decrease that rate by a factor $\sim 10^3$ and provide a larger (indeed a usable) AgKα/FeKα ratio. The need for this absorber renders use of silver L X-rays out of the question in the PIXE case.

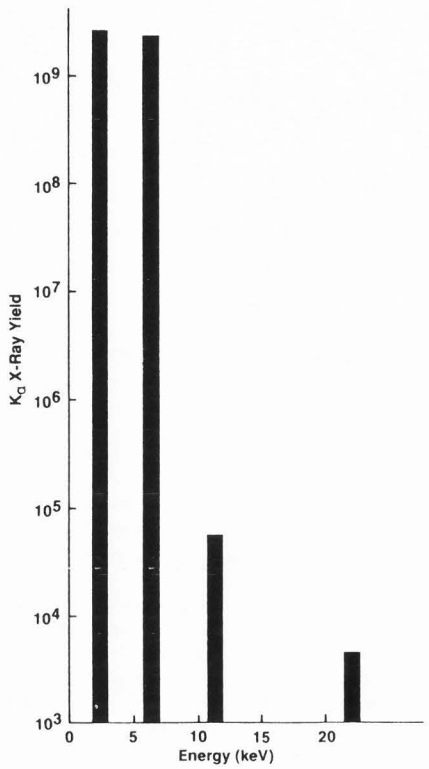

Fig. 1. Calculated PIXE spectrum of a pyrrhotite specimen (FeS) containing 100 ppm each of Se and Ag. Protons of 3 MeV energy are incident normal to the specimen and the X-ray take-off angle is 45°. X-ray intensity is per steradian and per microCoulomb of proton charge. Detector efficiency and lineshape and absorbing filters are ignored.

In PIXE then the X-ray energy region of interest typically runs up to ~30 keV. In turn, a knowledge of spectrometer response and background over an energy range twice that normally encountered in EPMA is required.

Representation of characteristic X-rays

The simplest approach, and one used widely in EPMA, is to record spectra ST(x) from single-element standards (x = channel number); the continuum background is removed from these (see below) and they are then stored on disk. This facilitates a linear least-squares fit of the sample spectrum SP(x) (containing contributions from i elements) which is represented by:

$$SP(x) = \sum_i a_i ST(x) + B(x) \qquad (1)$$

The background B(x) is either removed mathematically from the sample spectrum or given analytic representation. Then the fit is performed with the overall amplitudes a_i as the linear variables to be determined. Major advantages are the computational economy that accrues from working entirely with stored numeric arrays and from the

linear nature of the fit. Automatic inclusion of escape peaks and low-energy tailing in ST(x) is another advantage, somewhat offset by the error incurred by whatever technique is used to strip the background from the standard spectrum. The approach is very sensitive to any small shifts in energy-versus-channel calibration, making it advisable to renew the ST(x) data regularly. Another disadvantage is that the matrix attenuation of a given element's various X-ray lines differs between the specimen and the standard, placing a definite limitation on the quality of fit attainable. This can be a more serious drawback in PIXE than in EPMA, as exemplified in detail below.

These are two of the reasons why PIXE analysts have generally not espoused use of stored numerical spectra. Instead the majority have followed the second EPMA option of modelling the spectrum analytically. In the first approximation each line in a given element's spectrum is modelled by a Gaussian:

$$G(x) = H_G \exp\left[- \frac{(x-x_o)^2}{2\sigma^2} \right] \qquad (2)$$

and the centroids x_o and widths σ of the Gaussian are related to peak energy E_n of the n^{th} X-ray line by:

$$(x_o)_n = p_1 + p_2 \; E_n \qquad (3)$$
$$(\sigma^2)_n = p_3 + p_4 \; E_n \qquad (4)$$

Now the spectrum ST(x) of one element is a sum of Gaussians whose relative intensities must be constrained by an X-ray intensity data base. The specimen spectrum is the sum of the elemental spectra as in eq. (1). To obtain the amplitudes a_i, which are usually assigned as the height of the most intense peak for each element, a least-squares fit is done. If p_1 .. p_4 are accurately known they may be fixed at the known values, leaving only the peak height parameters as variables to be determined by the fit; a linear least-squares fit is then appropriate. However most PIXE workers have taken the view that if the computational overhead is to be expanded by adopting an analytic peak model, one might as well allow p_1 .. p_4 to be variables, which necessitates a non-linear fit. Indeed if B(x) is modelled using non-linear parameters, the fit already is a non-linear one. On modern microcomputers the resulting loss of speed does not appreciably extend the overall time for a PIXE analysis. The fact that small calibration drifts are now catered for automatically is an advantage.

This approach facilitates inclusion of the rather large PIXE matrix corrections (see below), which simply modify the relative intensities for the lines in each element's spectrum. The price paid is the need for a mathematical peak-shape model, and in practice the Gaussian is not an adequate approximation. Si(Li) detectors display significant low-energy tailing whose contribution relative to the parent Gaussian depends very strongly on energy. We have found (3) that the addition of one or two double Gaussian-convoluted exponential tails of the form:

$$D(x) = \frac{1}{2} H_D \exp\left[\frac{x-x_o}{\beta}\right] \mathrm{erfc}\left[\frac{x-x_o}{\sigma\sqrt{2}} + \frac{\sigma}{\beta\sqrt{2}}\right] \qquad (5)$$

provides an excellent description of our present Si(Li) device in the X-ray energy range 4-16 keV where the tailing is predominantly due to incomplete charge collection in the crystal; the parameters β and H_D, both of which are functions of energy, have to be measured independently. Recent work by Krumrey et al. (12) indicated that this function works well down to 1 keV energy. However it is not always appropriate at lower energy, and we recognize that the charge collection and the resultant tailing vary from one detector to another. The intensity of the charge collection tail decreases rapidly with increasing X-ray energy and in our detector it is negligible by 16 keV. Unlike EPMA, PIXE routinely generates spectra that extend to X-ray energies of ~30 keV. Above 20 keV, low-energy tailing starts to grow again, but it arises now from a different mechanism and has a different shape; a broad shelf of finite width left of each peak arises from Compton scattering of X-rays en route to the detector. We are presently working on a simple analytic form for this tailing phenomenon, based upon the known kinematics of the scattering process.

One main outcome of a round-robin intercomparison (2) of fitting techniques in PIXE was a recognition that a better understanding and description of the peak tailing due to both physical mechanisms was needed; in that work the largest variations among individual results occurred for weak peaks riding on the low-energy tails of intense peaks. While the tailing effects are identical in PIXE and EPMA, the consequences for analytic accuracy are more serious in PIXE because of the wider range of peak intensity that occurs in PIXE spectra. In the example of figure 1 a thin aluminum foil has to be interposed to attenuate preferentially the lower-energy X-rays of the matrix elements, but even then the matrix peaks are frequently several orders of magnitude more intense than the trace element peaks. This necessitates an accurate description of peak distortions even if they constitute less than 1% of the intensity. Figure 2 provides an example of an actual pyrrhotite spectrum containing peaks due to 1000 ppm concentrations of copper and palladium; a 0.25 mm aluminum absorber was used to reduce the matrix peak intensities.

Several other points are worth making. First the need to describe tailing in PIXE spectra adds further to computing time and complexity. Then it is not straightforward to extract the necessary accurate tailing information from normal X-ray spectra of pure elements due both to the multiplet nature of the spectra and to the presence of radiative Auger satellites. Accurate determination of tailing demands use of a source of monoenergetic X-rays tunable over the 1–30 keV range. Incidentally in this general context, it is interesting to note the excellent progress being made in fabricating HPGe detectors with much-reduced tailing relative to the previous generation (5). This may result in increased use of HPGe in PIXE, which to date has been dominated by Si(Li) detectors.

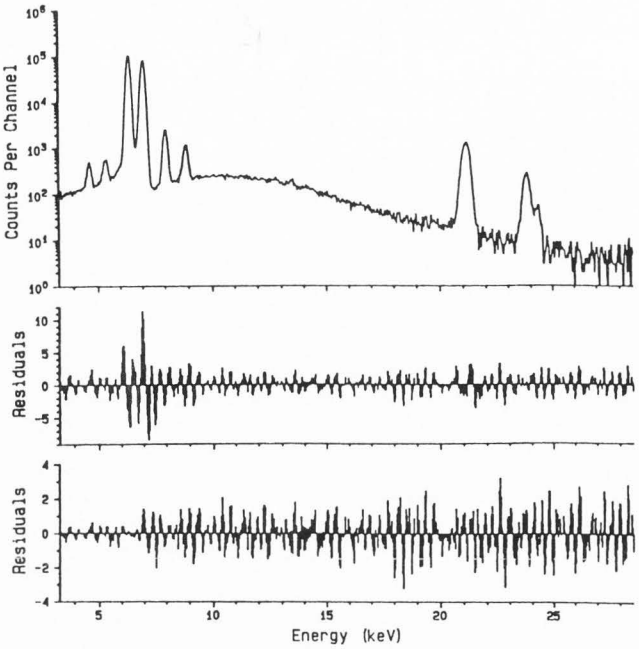

Fig. 2. Details of fits to a pyrrhotite (FeS) spectrum where Cu and Pd concentrations are each 100 ppm. The first set of residues results from normal weighting of the chi-squared using statistical errors only. The second set results from augmenting this weighting by the effect of a ±1% error in the attenuation coefficient of the 0.25 mm Aℓ filter. The residues are the differences between the top-hat-filtered model and measured spectra, in units of one standard deviation.

Matrix effects upon relative X-ray intensities

Matrix corrections are necessary both in spectrum fitting and in the conversion of X-ray intensities to concentrations via whatever standardization procedure is adopted. It is the first of these that concerns us here, and the concern arises because differential matrix attenuation of an element's various X-ray lines causes their relative intensities to differ from the data base values which would prevail in the limit of a very thin specimen. This is not important in a simple spectrum, such as that of fig. 2, where the principal peaks are free of overlaps, and their intensities can be extracted directly. It is very important in the case of crowded spectra where there is extensive overlap among the X-ray series of several elements. In these cases the least-squares fit proceeds by varying the height of the principal line of each element and maintaining all subsidiary line intensities in appropriate ratio computed from the data base with requisite matrix corrections.

To compare these matrix corrections to relative intensities in EPMA and μ-PIXE, we use the example of $K\beta/K\alpha$ X-ray intensity ratio of trace elements in an iron matrix.

In EPMA, $\phi(\rho Z)$ curves may be used to compare $K\beta/K\alpha$ for a specimen of the element itself and for the element in the iron matrix. This ratio is:

$$R = \frac{(K\beta/K\alpha)_Z \text{ (matrix Z)}}{(K\beta/K\alpha)_Z \text{ (matrix Fe)}} \qquad (6)$$

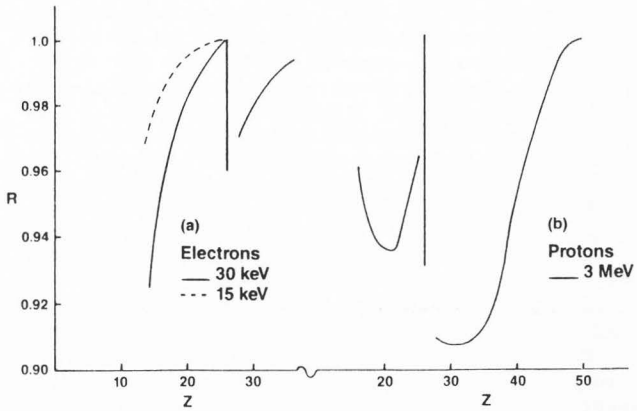

Fig. 3. Illustration of matrix effects in EPMA and PIXE. The quantity R (defined in the text) is plotted versus Z for electrons and protons of typical energies.

Figure 3(a) gives the R-values for electron energies of 15 and 30 keV (J.D. Brown, private communication) with normal incidence and 45° take-off angle. R departs significantly from unity only in the extreme case of very low-energy X-rays and deep electron penetration. In practice, the higher-energy electrons would be used to analyze elements having Z > 26 and here R is within 3% of unity (except for Co, where there is a differential absorption effect). For the very light elements, lower electron energies would be used and again this would keep R within 3% of unity. The matrix corrections are clearly quite small.

Figure 3(b) presents the R values for 3 MeV protons with normal incidence and 45° X-ray take-off angle; details of the calculation are discussed later. The general behaviour is very similar to the electron case, but the directions from unity are considerably larger. There are two reasons for this. The first is simply the much greater penetration of the protons. In EPMA the depth of analysis is almost always limited by the electron penetration, the main exception being X-rays of energy below 1 keV. Table 1 shows that a different situation pertains in PIXE. The proton range is often much greater than the attenuation length. Thus in both our examples, with the typically used 2–3 MeV energy protons, the latter determines the depth probed; 90% of the observed silicon K X-rays originate within 1–2 attenuation lengths of the surface, despite the proton reaching much greater depths. The exception in our example occurs for low proton energy in silicon, where range and X-ray attenuation length are similar and silicon has a high transmission for its own X-rays.

The second reason is the $K\beta$ satellite which arises from simultaneous ionization of the K and L shells. This satellite is of negligible intensity in EPMA but cannot be ignored in PIXE. We have discussed the satellite energies and intensities in detail elsewhere (14). For

Table 1.
Depth D_{90} above which 90 % of observed silicon K X-rays originate in a silicon matrix and an iron matrix.

Proton Energy (MeV)	D_{90} (μm)		X-ray attenuation length (μm)		Proton Range (μm)	
	Si	Fe	Si	Fe	Si	Fe
1	7.9	0.8	12.0	0.55	15.8	7.0
2	16.6	0.9			46.7	19.0
3	18.9	0.9			90.3	36.0

illustrative purposes we note here that at 3 MeV proton energy the intensity ratio of the satellite to its parent Kβ line decreases from 3% at Z=18 to 1% at Z=48, and at 2 MeV from 4% at Z=18 to 0.9% at Z=48. Although the 'satellite' actually comprises a plethora of closely-spaced transitions, it is our experience that addition of a single extra Gaussian to the model provides an adequate description. For elements having $Z \leq 29$ the energy displacement of the satellite above its parent line is large enough to place it just above the K absorption edge of the neutral atom. If a thick target contains a large concentration of an element whose $Z \leq 29$, the Kβ satellite of that element is then very strongly attenuated, with consequent decrease of the Kβ/Kα intensity ratio to the thin target line. This effect causes a significant decrease in the R value over and above the simple effect of differential attenuation of the principal Kα and Kβ lines. Unlike in the EPMA case the PIXE R value does not decrease monotonically but starts to increase again as Z falls past ~17.

The overall picture is that the matrix corrections to relative X-ray intensities in PIXE are much larger than in EPMA and must not be neglected. Fortunately the matrix correction is very straightforward to calculate in PIXE (10). The relative intensity of a particular line of element Z in a given matrix is modified relative to the "thin-target" value by the factor:

$$f = \int_{E_o}^{o} \frac{\sigma_z(E)\ T_z(E)}{S(E)}\ dE \qquad (7)$$

where E = proton energy (intial value E_o); $\sigma_z(E)$ is the energy-dependent ionization cross-section; S(E) is the matrix stopping power for protons (MeVcm^2 g^{-1}); and:

$$T_z(E) = \exp\left\{ -\mu_z \frac{\cos\alpha}{\sin\theta_{TO}} \int_{E_o}^{E} \frac{dE}{S(E)} \right\} \qquad (8)$$

where μ_z is the mass attenuation coefficient (cm^2 g^{-1}) of the X-ray of interest, α is the beam angle relative to the normal and θ_{TO} the X-ray take-off angle. The quantities S(E) and μ_z can only be evaluated if the concentrations of the major matrix constituents are known. In many applications of PIXE this is indeed the case (for example via stoichiometry or by prior use of EPMA) and the correction factors f are directly calculable. If the matrix is unknown, then an iterative solution of the X-ray yield versus element concentration equations is called for, with the spectrum fitting repeated each time the matrix is adjusted. Although time-consuming this is quite feasible.

Absorber effects upon relative X-ray intensities

In EPMA the only materials between specimen and detector are the detector window and its frontal attenuating layers, which have only small differential effects upon intensity ratios such as Kβ/Kα. We indicated earlier that it is frequently necessary in PIXE to interpose an absorber between the specimen and the detector. The schematic pyrrhotite spectrum of figure 1 illustrated why this is so. With typical counting rates (10^3 s^{-1}) and counting times (10^3 s) and the $>10^5$ yield ratio between Fe and Ag, the number of Ag Kα counts in an actual spectrum would be approximately 1. With a low Z absorber interposed to eliminate the sulfur X-rays and reduce the iron Kα by ~10^3 one can accumulate a few thousand Ag Kα counts; we use typically a 0.25 mm Aℓ absorber in this context.

The result of this absorber is to increase the iron Kβ/Kα ratio from its nominal value of 0.1356 by a factor of just over 5. Any small error in the assumed mass attenuation coefficients of aluminum or in the foil thickness will transmit error into the Kβ/Kα ratio of iron, whose peaks remain by far the dominant feature of the spectrum. This causes visible worsening of the goodness of fit as measured by the residuals between the measured and model spectra, and as illustrated in figure 2. An elegant compensation for this (1) is based on recognition that in the non-linear least-square fit, the difference between model and measured spectrum at each channel should be weighted not just by the statistical counting error but also by the estimated uncertainty in absorber transmission at the corresponding X-ray energy. In figure 2 the first set of residuals corresponds to the conventional weighting by statistical error. The second set reflects the linear addition to the statistical error of the error accruing from a ±1% uncertainty in the product of X-ray attenuation coefficient and aluminum foil thickness right across the spectrum; the result of this is localized in the iron K X-ray region and its effect is to bring the residuals there into consistency with the rest of the spectrum.

The Data base for PIXE spectrum modelling

Most PIXE analysts use the theoretical K and L

X-ray emission rates of Scofield (19), based on Hartree-Fock wave functions. These agree well with experimental data (10), the sole exception being the Z = 20–30 region where the 3d shell is filling. Some prefer to rely on a review (18) of experimental data. An advantage of the Scofield work is that it provides the intensities of radiative Auger satellites, which can reach a few percent of their parent line intensities. Given our earlier arguments on inclusion of peak tailing effects at the 1% level, the need to include RA satellites follows. Neither RA nor double ionization satellites are included in EPMA, but the double ionization satellite of $K\beta$ in PIXE constitutes several percent of its parent and is detectable in the fitting procedure. In our own software the PIXE K X-ray data base contains the energies and intensities of 4–6 K X-ray lines, including satellites. The relative intensities appear accurate to within ±1% for the diagram lines.

The L X-ray case is less satisfactory. Accurate intensity ratios for the ~20 lines depend on knowledge of subshell ionization cross-sections, Coster-Kronig and fluorescence yields, and finally subshell emission rates. Uncertainties in the $L\beta/L\alpha$ and $L\gamma/L\alpha$ ratios are 5–10%; for individual L lines the uncertainties are much higher (10).

The matrix effect calculation demands ionization cross-sections, stopping powers and X-ray attenuation coefficients. We intend to discuss the accuracy of this data base in detail elsewhere, but can estimate that f values are accurate to within 5% in general for K X-rays.

The Continuum Background in PIXE

In EPMA the background is due to bremsstrahlung emitted by the decelerating electrons. It may be modelled by various relatively simple expressions based on the original Kramers expression (11), which is now known to underestimate the continuum intensity at low X-ray energies, and which neglected the Z-dependence of the background shape. The various modified forms contain corrections for these shortcomings (20). A modified Kramers continuum may be incorporated in a least-squares fit via a single overall intensity parameter. Alternatively further parameters may be varied by the fit to optimize the background shape, as in the FRAME C background (16):

$$B(E) = \frac{b_1(E_o-E)}{E} + \frac{b_2(E_o-E)^2}{E} \qquad (9)$$

where E_o = electron energy, E = photon energy and the variables are b_1 and b_2. Whatever the expression, it has to be corrected both for detector efficiency and for absorption within the specimen.

The PIXE background is much more complex, because there are several different contributors, viz., secondary electron bremsstrahlung (SEB), atomic bremsstrahlung (AB), radiative ionization (RI), nuclear bremsstrahlung, and gamma radiation from proton-induced nuclear reactions. The relative admixture of SEB, AB and RI depends upon target atomic number and proton energy, and once these are defined it varies across the X-ray energy spectrum. Full theoretical descriptions of these three atomic processes have been given by Ishii and Morita (8). These three components all have a very steeply decreasing dependence on X-ray energy (see figure 4) and a full description of thick-target background would call for incorporation of matrix absorption and detector efficiency. The much higher energy gamma radiation interacts via the Compton effect in the detector, leaving an essentially flat continuum unaffected by these two factors.

Given this complexity it is not surprising that little progress has been made towards a universal background expression of the Kramers type. Instead PIXE workers have used either empirical models or have resorted to mathematical techniques that remove background without the need for specific assumptions regarding its form.

Analytical Model

The term common to essentially all models (1,2,4,7,9,13,14,21) is an exponential polynomial which describes the bremsstrahlung background; orders up to 6 have been cited and in some cases the order (k) is left to the discretion of the user of the program. This expression has to be multiplied by an energy-dependent factor T which describes the transmission through absorbing foils, the detector window and its frontal attenuating layers, etc. In contrast, gamma-ray background arises from photons of high enough energy that the resulting spectrum is unaffected by absorbers, and is almost flat; it is usually represented by a constant, but sometimes a term exponential or inverse in channel number is added to provide for slight curvature. Finally some workers include a term to describe any contribution from noise at the extreme low-energy end of the spectrum; this is usually a rapidly decreasing exponential. If all these are included we have:

$$B(x) = B_{BREM}(x) + B_{GAM}(x) + B_{NOISE}(x) \qquad (10)$$

Where

$$B_{BREM}(x) = T\ B_{10}\ \exp\left[\sum_{k=1}^{\leq 6} B_{1k}\ (x-x_c)^k\right] \qquad (11)$$

$$B_{GAM}(x) = B_{20} + B_{21}\ \exp[B_{22}\ (x-x_c)] \qquad (12)$$

$$B_{NOISE}(x) = B_{30}\ \exp\left[B_{31}\ (x-x_c)^{B_{32}}\right] \qquad (13)$$

and the relationship between photon energy E and channel number x is given by eq. (3); x_c is usually chosen as the central channel of the region.

It is rare to find all these terms incorporated and usually k is chosen as less than 6; the narrower the energy region the smaller the necessary value of k. Even so the number of parameters to be determined is much larger than in the EPMA case (eq. 9). This can result in negative intensity parameters emerging from the fitting procedure, a problem that can be handled by constraining both the parameters and X-ray peak height parameters to be positive. Another problem with an exponential polynomial is its propensity to be driven quickly to infinite values by quite small

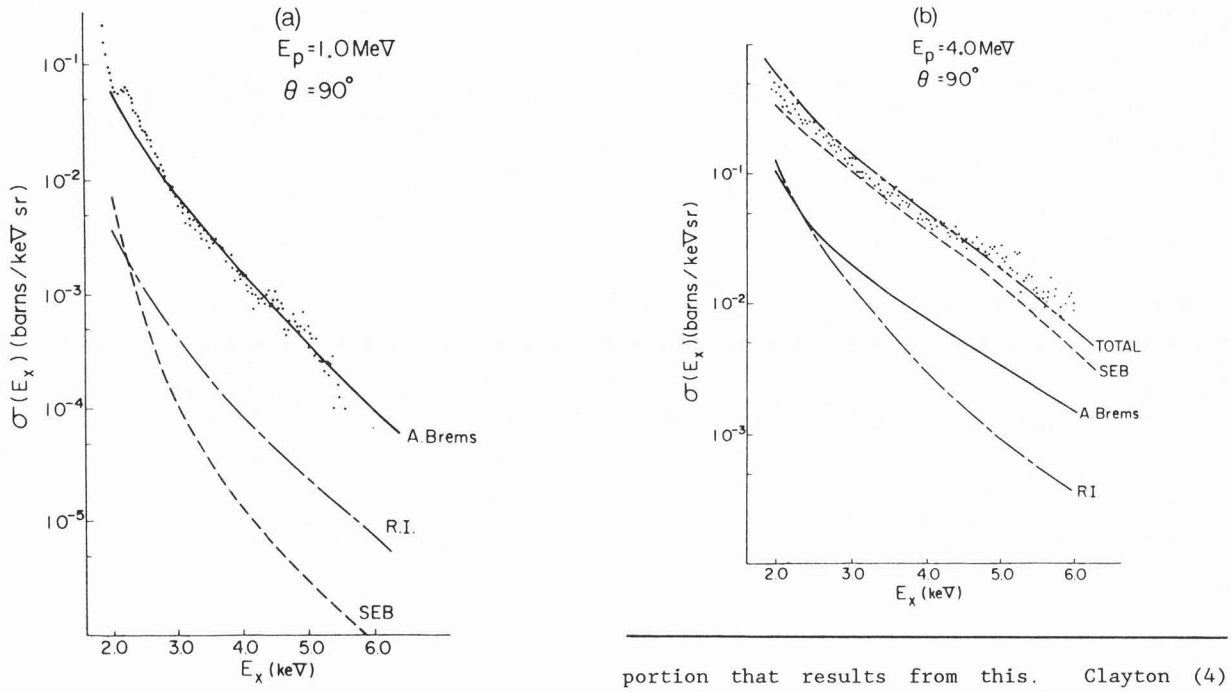

Fig. 4. Theoretical and measured continuum X-ray spectra for protons incident on a thin aluminum target (8). Reproduced by permission of the American Physical Society.

changes in the high-order parameters, with the result that the fit is aborted. A simplification sometimes adopted is to determine some of the background parameters (e.g., the polynomial coefficients) for a given specimen type through a few high-statistics measurements; these are then fixed and only the intensity coefficients B_{10}, B_{20}, B_{21}, B_{30} allowed to vary in the fitting of the main suite of spectra. Clayton's program (4) provides an elegant and flexible approach in this context; he divides the measured spectrum by T to remove the strong curvature (figure 5) and then smooths and differentiates it to locate local minima; next the logarithms of these data points are fitted to a polynomial to provide the parameter set B_{1k}. He then returns to fitting the raw spectrum and offers the options:– (i) the background is fixed as determined; (ii) the background may be scaled in overall height; (iii) the B_{1k} may be further varied.

One further point concerns discontinuities in the model B(x). These are introduced by the factor T at the Si K and Au L absorption edges, and also, if T properly includes X-ray self-absorption in a thick specimen, at the absorption edges of the matrix elements. Some but not all authors explicitly indicate that the latter effect is included in T. These discontinuities are not present in the experimental data, due to finite resolution, and so in the model it is appropriate to reach the same effect by convoluting B(x) with a Gaussian whose width is given by eq. (4).

Background removal

The major alternative to fitting model backgrounds is to strip away the background by some mathematical technique prior to fitting the peak portion that results from this. Clayton (4) describes an algorithm which examines the height Y_x compared to the average of the heights Y_{x-1} and Y_{x+1} on either side; if Y exceeds 0.5 (Y_{x-1} + Y_{x+1}) it is replaced by the mean; after 700 passes through the spectrum an acceptable background is left. This background is not quite as smooth as the polynomial background but has always been usable. Maxwell et al (14) have adopted for PIXE the top-hat filtering technique that is widely used in EPMA (15). This filter when convoluted with a spectrum (see figure 6) eliminates any linear portion; it essentially replaces the spectrum by its curvature at any point. Its use on real spectra is thus predicated on the assumption that the background is linear over the typical filter width of 200–500 eV. If absorbers are used to reduce the bremsstrahlung this is a reasonable approximation, and it has the advantage of avoiding any algebraic assumptions regarding background shape. It is no more economic than the modelling alternative however, since the large reduction in variables to be fitted is offset by the time taken to convolute the model in every iteration of the fitting procedure.

In the filter method background steps at absorption edges play no role. The most direct way to include them is to incorporate analytical step functions in the peak model, placing these at the absorption edges of the major matrix elements together with gold and silicon.

Linear approximation

A very simple approach based again on the assumption that the background is linear over short intervals is to locate local minima and join them by straight line segments. The accuracy will depend strongly on the proximity of the minima. The proponents (7) found at most 3% difference relative to the background produced by Clayton's iterative method (4); the context was thin specimens of amniotic fluid on Mylar substrates.

SNIP Procedure

The final background treatment to be noted is

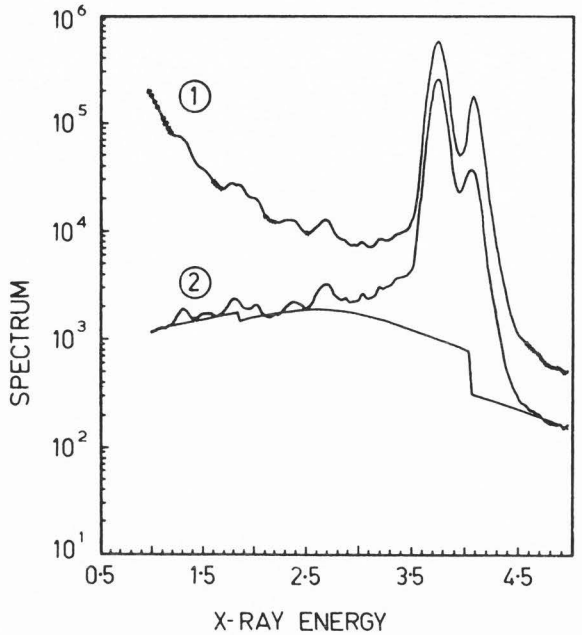

Fig. 5. A simple PIXE spectrum [1] after division by the detector efficiency and self-absorption corrections. [2] the resulting background polynomial displayed on the (displaced) original spectrum. Reproduced from ref. (4) by permission of the author.

yet another response to PIXE's unique problem of presenting a very wide range of peak heights (up to 10^6:1) in a given spectrum. It is often desirable to reduce the statistical fluctuations in low-intensity regions, usually by an n-point mean process, before fitting or removing background. However if this is done it raises the minima between closely-spaced peaks in high-intensity regions. In the example of figure 7 the weak nickel Kα peak is smeared into the very intense neighboring iron Kβ peak. The very weak peaks at high energies are likely to be overestimated due to the smoothing, and indeed multiple analyses of a specimen using integrated beam charges varying by a factor 100 result in fitted intensities per unit beam charge which display a dependence upon the integrated beam charge.

Ryan et al (17) have devised a special n-point digital filter which processes a spectrum in one pass, examining the region around each channel, and adapting both the smoothing interval and the degree of smoothing to confine the effect to low-statistics regions without being influenced by the flanks of intense peaks. The result, shown in figure 7, is superior to a conventional 7-point smooth.

This smoothing is the first part of a 3-stage statistics-sensitive non-linear iterative peak-clipping procedure (SNIP). After the smoothing (phase 1) the dynamic range of the spectrum y(x) (typically 0 - 10^7) is compressed to 0 - 2.8 by the transformation:

$$Z = \log[\log(y+1) + 1] \qquad (14)$$

Then each channel value Z(x) is replaced by the lesser of $\underline{Z}(x)$ and the mean $\overline{Z}(x,w)$ where:

$$\overline{Z}(x,w) = 0.5[Z(x+w) + Z(x-w)] \qquad (15)$$

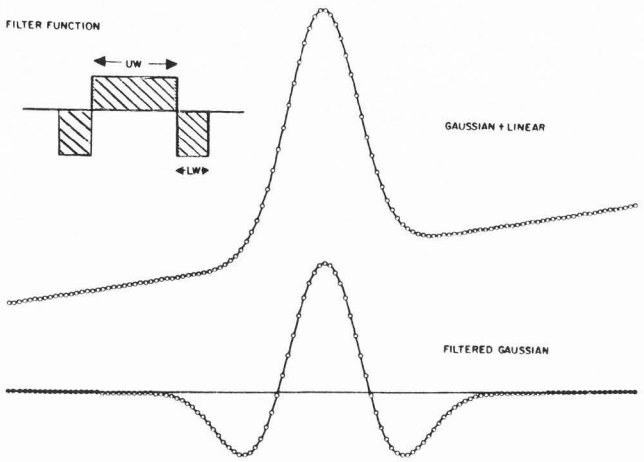

Fig. 6. Application of a top-hat filter to a pure Gaussian peak superimposed on a linear background.

and w(x) is twice the full-width-half-maximum value at channel x. About 24 iterations through this peak suppression procedure suffice to reduce the spectrum to an acceptable background. For the last few passes, w is successively reduced in order to minimize oscillations. Finally the inverse transformation to eq. (14) restores the background to counts per channel.

This approach has been intensively tested using USGS rock standards. Agreement of measured and certified trace element concentrations, illustrated in Table 2 for the United States Geological Survey AGV-1 rock standard, lends it strong support.

Peak-Fitting Inter-Comparison

We have shown that extant procedures for fitting PIXE spectra have a fairly standard approach to treating characteristic X-ray peaks but employ a wide variety of approaches to the continuum background. Subsidiary aspects such as peak pile-up are dealt with in refs. 1,2,4,10,13,14,21. There are also slight differences in the data bases used in the various treatments. It is therefore very encouraging that a spectrum-fitting inter-comparison carried out by five groups (2) resulted in excellent agreement among the peak areas for trace and minor elements extracted by their computer codes from a set of PIXE spectra recorded using biological, geological and environmental samples. Space limitations preclude a complete reprise of these results but several general comments can be made.

For single-element standards, the Kα peak intensities agreed at the 1% level except for $Z < 20$ and $Z > 40$. For $Z < 20$ the tailing arises from charge losses in the detector (3) while for $Z > 40$ it results from X-ray scattering en route to the detector. The need for improved analytic description of peak tailing in both these regimes was also demonstrated in the twelve specimen spectra. Averaging over the Kα peak areas P of all elements (9-18 per spectrum) in all twelve spectra, and restricting the data to those whose mean reported intensities exceeded the determination level (6), the results are as in

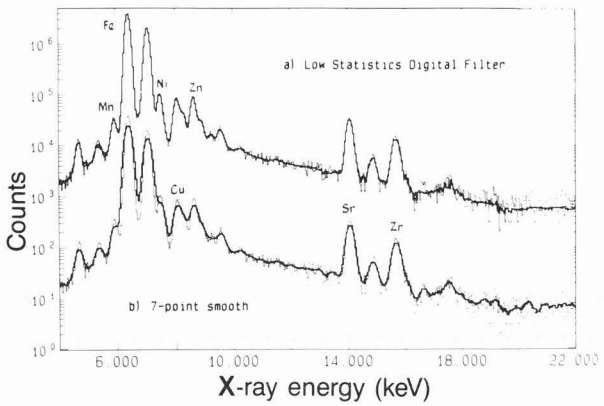

Fig. 7. PIXE spectrum from a mineral grain processed (a) with the low-statistics digital filter of ref. (17); (b) with a 7-point mean smoothing. (The two spectra are offset by x100.) Reproduced by permission of Elsevier Science Publishers (Physical Sciences and Engineering Division).

Table 3. The overall spread in the average value of $P/\bar{P}$ ($\bar{P}$ is the system mean for a given element in a given spectrum) is a little over 5%. Much of the spread is due to a few cases where very weak peaks ride on the low-energy tails of very intense peaks, e.g., the Cr and Mn Kα lines superposed on the Fe Kα tail in spectra containing strong iron peaks; in these cases spreads of up to 35% were observed.

This tailing problem is of more importance in PIXE than in EPMA. The lower background results in an increased sensitivity to fine details of peak shape such as low-energy tailing. More work is needed on the tailing phenomenon.

Most of the programs tested in the inter-comparison have since undergone changes which would significantly improve the results in Table 3. The first group has reprocessed the data using a polynomial background instead of iterative stripping (4); its result improves from 0.969 to 1.0103 (parameters varied) or 1.003 (parameters fixed). Improvements also would be likely for other participants; for example the code of the second group lacked matrix corrections, which are now incorporated (14). The third participating group has contributed further commentary (13) which is an important postscript to the exercise.

Given the extensive developments since this inter-comparison (conducted in 1984/5) and the growing use of PIXE and μ-PIXE, a further such exercise demanding complete analysis (i.e., reporting peak areas and concentrations for thick specimens) would seem timely. This should be focussed upon recognized standard reference materials.

Concluding Remarks

Finally, since the present paper has focussed mainly on methodology, fig. 8 presents a typical PIXE spectrum encountered in our own mineralogical work, together with the residues of a least-squares fit done with our software. The spectrum and the

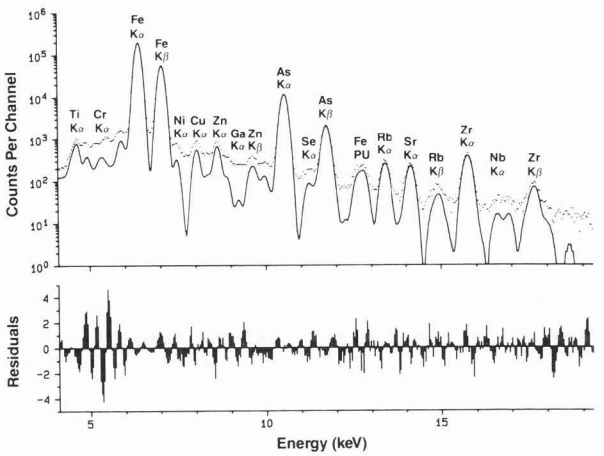

Fig. 8. Details of fit to the PIXE spectrum of a quartz mineral. The residues are defined as in fig. 2.

Table 2. PIXE analysis of U.S.G.S. AGV-1 rock standard (17).

Element	Concentration (ppm) PIXE (± 1σ)	Accepted values
Mn	822 ± 10	775
Fe (%)[a]	(4.7)	4.7
Ni	14.2 ± 1.2	16
Cu	59.5 ± 1.2	60
Zn	91.7 ± 2.3	86
Ga	21.4 ± 1.0	20.5
Pb	36.4 ± 2.1	35
Th	5.6 ± 1.6	6.5
Rb	75.0 ± 1.8	67
Sr	703 ± 13	660
Y	20.4 ± 1.4	20.5
Zr	241 ± 9	225
Nb	13.4 ± 1.8	15
Ba[b]	1146 ± 50	1210

[a] The PIXE analysis was normalized to the accepted iron value, i.e., iron was used as an internal standard.

[b] Some inhomogeneity in barium was observed.

Table 3. Integrated results of the PIXE fitting inter-comparison [4], expressed as the average value of $P/\bar{P}$. P is the peak area for a given element in a given spectrum and $\bar{P}$ the mean of P over the five groups reporting. $P/\bar{P}$ is then averaged for each group over all elements in all spectra.

Group	Mean $P/\bar{P}$
1	0.969
2	1.005
3	0.987
4	1.012
5	1.028

Table 4. Concentrations measured in quartz spectrum of figure 8

Element	Concentration (ppm)	Detection Limit
Ti	1450 ± 180[a]	360
Cr	27 ± 11	23
Mn	88 ± 6	11
Fe	15 800 ± 20	6
Ni	13.6 ± 1	1.6
Cu	21.8 ± 1	1.3
Zn	24.6 ± 1	1.1
Ga	1.1 ± 0.5	1.0
As	574 ± 3	1.7
Se	4.2 ± 0.6	1.1
Rb	20 ± 1	2.0
Sr	29 ± 1	1.3
Zr	79 ± 2	2.2
Nb	5.1 ± 1.6	3.8

[a] The error estimates produced by the least-squares fitting software (15) are in units of one standard deviation

concentrations (Table 4) reinforce many of the points made in this paper regarding spectrum fitting. PIXE responds here to a concentration range (1.1 ppm Ga to 0.16% Fe) that results in a dynamic range of peak intensity nearly 10^5:1 even with a 0.25 mm aluminum absorber present. Peak overlaps are extensive, demonstrating the need for accurate relative X-ray intensities and corresponding matrix corrections. Weak peaks (Cr,Ti) ride on the low-energy tails of intense peaks (Fe), showing the need for a good description of tailing. The quality of the residue spectrum indicates that these aspects are being coped with acceptably well. Nonetheless further work on all aspects is merited.

Acknowledgement

This work is supported by the Natural Sciences and Engineering Research Council of Canada. My thanks are due to J.A. Maxwell and W.J. Teesdale.

References

(1) Benjamin TM, Duffy CJ, Rogers PSZ, (1988) Geochemical utilization of nuclear microprobes. Nucl. Instrum. Meth. B30, 454-458.

(2) Campbell JL, Maenhaut W, Bombelka E, Clayton E, Malmqvist K, Maxwell JA, Pallon J, Vandenhaute J (1986) An intercomparison of spectral data processing techniques in PIXE. Nucl. Instrum. Meth. B14, 204-220.

(3) Campbell JL, Perujo A, Millman BM (1987) Analytic description of Si(Li) spectral lineshapes due to monoenergetic photons. X-Ray Spectrom. 16, 195-201.

(4) Clayton E (1986) PIXAN: The Lucas Heights PIXE analysis computer package: Australian Atomic Energy Commission Report M113.

(5) Cox CE, Love BG, Sareen RA (1988) Small area high purity germanium detectors for use in the energy range 100 eV to 100 keV. Application Note (Link Analytical Ltd., UK).

(6) Currie LA (1968) Limits for qualitative detection and quantitative information. Anal. Chem. 40, 586-592.

(7) Gertner I, Heber O, Zajfman J, Zajfman D, Rosner B (1989) Comparison between two computer codes for PIXE studies applied to trace element analysis in amniotic fluid. Nucl. Instrum. Meth. B36, 74-81.

(8) Ishii K, Morita S (1984) Continuum X-rays produced by light ion-atom collisions. Phys. Rev. A30, 2278-2286.

(9) Johansson GI (1982) Modifications of the HEX program for fast automatic resolution of PIXE spectra. X-Ray Spectrom. 11, 194-200.

(10) Johansson SAE, Campbell JL (1988) PIXE: a Novel Technique for Elemental Analysis (John Wiley, Chichester, UK), 96-97.

(11) Kramers HA (1923) On the theory of X-ray absorption and the continuous X-ray spectrum. Phil. Mag. 46, 836-871.

(12) Krumrey M, Tegeler E, Ulm G (1989) Complete characterization of a Si(Li) detector in the photon energy range 0.9–5 keV. Rev. Sci. Instrum. in press.

(13) Maenhaut W, Vandenhaute J (1986) Accurate analytic fitting of PIXE spectra. Bull. Soc. Chim. Belg. 95, 407-418.

(14) Maxwell JA, Campbell JL, Teesdale WJ (1989) The Guelph PIXE software package. Nucl. Instrum. Meth. in press.

(15) McCarthy JJ, Schamber FH (1979) Least-squares fit with digital filter: a status report, Special Publication 604 (National Bureau of Standards, Washington DC).

(16) Myklebust RL, Fiori CE, Heinrich KFJ (1979) FRAME C: A compact procedure for quantitative energy-dispersive electron probe X-ray analysis, Nat. Bur. Stands. Tech. Note 1106 (Dept. of Commerce, Washington, DC).

(17) Ryan CG, Clayton E, Griffin WL, Sie SH, Cousens DR (1988) SNIP, a statistics-sensitive background treatment for the quantitative analysis of PIXE spectra in geoscience applications. Nucl. Instrum. Meth. B34, 396-402.

(18) Salem SI, Panossian SL, Krause RA (1974) Experimental K and L relative X-ray emission rates. At. Data Nucl. Data Tables 14, 91-109.

(19) Scofield JH (1974) Exchange correction of K X-ray emission rates. Phys. Rev. A9, 1041-1048.

(20) Scott VD, Love G (1983) Quantitative electron-probe microanalysis, (Ellis-Harwood, Chichester, UK).

(21) Zolnai L, Szabo' Gy (1988) PIXASE: A computer package for evaluation of PIXE spectrum series. Nucl. Instrum. Meth. B34, 118-121.

Discussion with Reviewers

D.E. Newbury: From your accumulated experience in testing PIXE quantitation procedures on known samples, can you make statements on the expected accuracy of a PIXE analysis for the following concentration ranges:
> 10% (Major)
0.1 – 10% (Minor)
< 0.1% (Trace)

Author: This is a very broad question meriting a full paper to deal with adequately. For a major element the uncertainty depends on whether it is subject to secondary fluorescence excitation. For

minor and trace elements the 'interference-free' uncertainty can be much worsened by peak overlap with major elements.

Our experience for major elements in NIST standard reference materials using the K-ratio method is typical accuracies of ±2%. But when an X-ray lies just above an absorption edge, this can double.

For minor elements we quote two examples. SRM 1159 (FeNi) alloy has 0.3% Mn; with 1 MeV protons we measured 0.28% and 0.31% at different points on the specimen. SRM 1261a (steel) has 0.69% Cr, and there is strong secondary fluorescence of Cr by Fe; here we measure 0.74 and 0.72%, i.e., the accuracy worsens to >5%. Much more work is needed on minor elements.

For trace elements the extensive study of 15 SRMs by W. Maenhaut, J. Vandenhaute, H. Duflou (Fres. Z. Anal. Chem. 326, 736-738, 1987) is very valuable. The authors emphasize that overall accuracy depends on calibration, beam-handling, specimen preparation, specimen homogeneity, contamination control, spectral data processing and matrix corrections. They utilized concentration data with error from counting statistics of under 15% and for each element they averaged over several specimens (prepared by different methods) and all materials. They conclude that the accuracy is somewhat better than 5%.

D.E. Newbury The real strength of the EPMA method is the determination of the ratio of intensities for an element in the sample and in a standard which is often a pure element. By measuring this ratio and calculating matrix corrections to the ratio, the need for absolute accuracy in a number of key parameters, especially the ionization cross section and fluorescence yield, is avoided. Perhaps I have misinterpreted your paper, but it seems to me that your quantitative method is much more dependent on having an accurate absolute cross section. What is the role of standards in quantitative PIXE analysis?

Author: This comparison method based on pure element standards (K-ratio method) is equally applicable in PIXE and is quite widely used, precisely because of the cancellation of the uncertainties in key parameters. We have discussed this in detail elsewhere [J.L. Campbell and J.A. Cookson, Nucl. Instr. Meth. B3 (1984) 185-197 and ref. (10)]. Because the projectile-target interaction is much simpler in PIXE [straight path, negligible backscattering] there exist simple accurate analytical descriptions of all quantities needed to evaluate the matrix corrections, hence the computation of these is fast and accurate.

In the above method one runs a pure element standard corresponding to every element of interest in the specimen, and interpolates where standards are not available. However in PIXE, X-ray production cross-sections at 1–4 MeV proton energies are known with ~2% accuracy, and so a single elemental standard can provide the complete calibration for a wide range of elements. In our own analyses of sulfide minerals we find that either a pure palladium standard or a synthetic mineral standard containing palladium provides an accurate overall standardization for elements in the range $26 \leq Z \leq 52$ in a range of different sulfide matrices; this conclusion was drawn by running an entire suite of standards in that range.

PIXE then is intrinsically no more dependent than EPMA on having accurate absolute cross-sections. But because very accurate cross-sections have recently become available, PIXE can take advantage of these to simplify the calibration procedure.

We will elaborate in detail elsewhere on the merits and defects of various PIXE standardization techniques in the context of the currently available data base.

J.D. Brown: For background removal and peak stripping, absorption by the specimen must be and usually is considered in EPMA. Accurate correction for this is widely available as a consequence of the work done with wavelength spectrometers. A discussion of EDS in EPMA can be found in P.J. Statham X-Ray Spectrometry **5**, 154 (1976) and **5** 16 (1976).

Because X-rays are generated more deeply in the specimen in PIXE, absorption effects must be much stronger and as can be seen in Figure 3, the higher continuum shelf to the left of the Fe peaks is just such an effect.

Author: I agree that, for example, absorption of iron X-rays in an iron specimen is greater in PIXE than in EPMA. But this is not the main cause of the continuum "shelf" seen in fig. 3. What is seen left of the peak is mainly secondary bremsstrahlung, much attenuated by the aluminum absorber; the intrinsic low-energy shelf due to incomplete charge collection in the Si(Li) detector is a minor contributor. The shelf is not strongly augmented by scattering in thick targets, because the energy loss in inelastic scattering is very small at energies < 10 keV